J. Earth Syst. Sci. (2020)129 77
https://doi.org/10.1007/s12040-020-1346-8

Observed variability of the East India Coastal Current on the continental slope during 2009–2018

S Mukhopadhyay[1,2], D Shankar[1,2,*], S G Aparna[1], A Mukherjee[3], V Fernando[1], A Kankonkar[1], S Khalap[1], N P Satelkar[1], M G Gaonkar[1], A P Tari[1], R R Khedekar[1] and S Ghatkar[1]

[1] *CSIR-National Institute of Oceanography, Dona Paula, Goa 403 004, India.*
[2] *Academy of Scientific and Innovative Research (AcSIR), CSIR-NIO, Goa 403 004, India.*
[3] *ESSO-Indian National Centre for Ocean Information Services, Hyderabad, India.*
**Corresponding author. e-mail: shankar@nio.org*

MS received 13 July 2019; revised 2 December 2019; accepted 3 December 2019

We describe the variability of the East India Coastal Current (EICC) during 2009–2018 using data from ADCP (acoustic Doppler current profiler) moorings deployed on the continental slope in the western Bay of Bengal. The four moorings are deployed off Gopalpur ($\sim$19.5°N), Visakhapatnam ($\sim$18°N), Kakinada ($\sim$16°N), and Cuddalore ($\sim$12°N) on the Indian east coast. The longer data record allows us to attach a statistically more robust basis to the conclusions drawn by Mukherjee *et al.* (2014) on the basis of four years (2009–2013) of ADCP data. The data confirm that the seasonal cycle dominates the variability of the EICC. The amplitude of the annual band varies over the time series. In the intra-annual band, the variability switches between the semi-annual and 120-day bands off Gopalpur, Visakhapatnam and Kakinada, but the semi-annual band is stronger than the 120-day band off Cuddalore throughout the time series. Upward phase propagation is common in the seasonal bands, but downward phase propagation is common in the intra-annual band off Cuddalore during the summer and winter monsoons, leading to stronger undercurrents there. Off Cuddalore, even the annual EICC appears as a shallow current. In contrast, the EICC appears as a deep flow off Gopalpur, Visakhapatnam, and Kakinada particularly during the spring inter-monsoon. This deep flow is evident at these locations even in the intraseasonal (30–90-day) band; the longer data set suggests, however, that the intraseasonal variability does not necessarily peak during spring. The annual EICC is coherent along the coast, but it is only the semi-annual band that shows a comparable coherence between Kakinada and Cuddalore: in the 120-day and intraseasonal bands, the EICC decorrelates along the coast. Wavelet analysis suggests significant variability at sub-annual periods. The sub-annual EICC exceeds 20 $\mathrm{cm\,s^{-1}}$ on many occasions, but it too decorrelates along the coast. The long ADCP record allows us to confirm the dominance of seasonality in the EICC regime in a robust fashion; the data show that the EICC tends to flow in its canonical poleward (equatorward) direction during spring (winter). This dominance of seasonality enhances the predictability of the EICC.

Keywords. Western boundary currents; ADCP; seasonal variability; intraseasonal variability; interannual variability; EICC; Bay of Bengal; Indian Ocean.

Published online: 20 February 2020

1. Introduction

The East India Coastal Current (EICC), which is the western-boundary current of the Bay of Bengal (usually called just 'bay' hereafter), reverses seasonally in response to the seasonally reversing monsoon winds (Shetye *et al.* 1991, 1993, 1996; Shetye and Gouveia 1998; Schott and McCreary 2001; Durand *et al.* 2009; Mukherjee *et al.* 2014). This seasonal variability was documented in the 1990s using ship-drift (Cutler and Swallow 1984; Mariano *et al.* 1995), hydrographic (Shetye *et al.* 1991, 1993, 1996), and sea-surface-temperature (SST; Legeckis 1987) data. The results of these and other studies are summarised in a few reviews (Varkey *et al.* 1996; Shetye and Gouveia 1998; Schott and McCreary 2001).

The ship-drift climatologies and hydrographic data show that the EICC flows poleward during February–September (Shetye *et al.* 1991, 1993) and equatorward during November–January (Shetye *et al.* 1996). The period of poleward flow consists of two parts, with the EICC being stronger and deeper during March–April, when it constitutes the western-boundary current of a seasonal gyre in the bay, and weaker and shallower during the summer monsoon (June–September), when a basin-wide gyre is not evident. Model studies show that the stronger EICC during March–April, when the winds over the bay are weak, is forced largely by the anticyclonic Ekman-pumping or wind-curl field over the basin (Shetye *et al.* 1993; McCreary *et al.* 1993, 1996; Shankar *et al.* 1996; Vinayachandran *et al.* 1996). A poleward EICC is forced by local winds blowing along the western boundary of the bay during the summer monsoon, but an opposing flow forced by cyclonic Ekman pumping over the basin and the winds over the equatorial Indian Ocean during May (Potemra *et al.* 1991; Yu *et al.* 1991; McCreary *et al.* 1993, 1996; Vinayachandran *et al.* 1996) weakens the poleward surface current, below which an undercurrent flows equatorward (Shetye *et al.* 1991; McCreary *et al.* 1993, 1996; Vinayachandran *et al.* 1996). The winds along the eastern boundary of the bay strengthen the equatorward flow (McCreary *et al.* 1996). Hence, the seasonal cycle of the EICC is forced by both local (alongshore) and remote (eastern boundary of the bay, equatorial Indian Ocean, and Ekman pumping over the basin) winds.

Its obvious importance for the local climate (see, for example, Shenoi *et al.* 2002) led to more investigations when satellite altimetry provided a near-synoptic view of the basin-scale circulation in the bay. Apart from confirming the hypothesis that a seasonal sub-tropical gyre exists in the bay during March–April and the EICC forms its western-boundary current at this time, the satellite data show that such a basin-scale gyre does not exist during the summer monsoon (Eigenheer and Quadfasel 2000; Shankar *et al.* 2002). The satellite data confirm (Durand *et al.* 2009; Kurien *et al.* 2010; Nuncio and Kumar 2012; Chen *et al.* 2012) the finding, based on hydrographic data of the summer–monsoon (Shetye *et al.* 1991), that the EICC consists of several eddies. The EICC decorrelates along the coast at both interannual and intraseasonal time scales and it is only the seasonal EICC that is coherent along the coast (Durand *et al.* 2009). The satellite revolution has also led to the creation of the gridded OSCAR (Ocean Surface Current Analysis Real-time) data set on near-surface currents based on altimeter and other satellite data (Bonjean and Lagerloef 2002).

In spite of this success of satellite altimetry, it has limitations, of which the most important, perhaps, is that the current is still an estimate, not a direct measurement. Direct current measurements in the Indian Exclusive Economic Zone (EEZ) were few and of short duration until the CSIR-National Institute of Oceanography deployed ADCP (acoustic Doppler current profiler) moorings on the continental slope and outer shelf off the Indian west (Amol *et al.* 2014; Amol 2014) and east (Mukherjee *et al.* 2014; Mukherjee 2017) coasts in October 2008 and April 2009, respectively. Mukherjee *et al.* (2014) used the ADCP data during 2009–2013 from the continental slope to describe the seasonal and intraseasonal variability of the EICC. In the regime of the EICC, seasonal variability is stronger than intraseasonal variability, a finding in contrast to the strong intraseasonal variability seen off the Indian west coast (Vialard *et al.* 2009; Amol *et al.* 2014). The ADCP data show that the seasonal cycle consists of the annual and semi-annual cycles, which were evident in the climatological EICC as well (Shankar *et al.* 1996), and variability in a band around 120 days (Mukherjee *et al.* 2014, 2018). Model simulations show that the observed annual cycle is largely driven by the local alongshore winds and Ekman pumping over the bay, with the asymmetry of the monsoon (McCreary *et al.* 1996) and equatorial forcing contributing to the semi-annual cycle (Mukherjee *et al.* 2018). The 120-day

variability has been discussed earlier for both West India Coastal Current (WICC) and EICC (Nethery and Shankar 2007; Han *et al.* 2011; Cheng *et al.* 2013; Girishkumar *et al.* 2013), but the process forcing this band is unclear (Mukherjee *et al.* 2018). The simulations also show that the influence of equatorial forcing declines in the intraseasonal band from north to south along the western boundary of the bay, with the local alongshore winds playing a more significant role in the south (Mukherjee *et al.* 2018). The ADCP data also confirm the result from satellite altimetry (Durand *et al.* 2009) that the EICC decorrelates along the coast at intraseasonal time scales (Mukherjee *et al.* 2014).

Upward phase propagation, a sign of remote forcing, is striking at all three moorings (Gopalpur, Kakinada, and Cuddalore; see figure 1) in the ADCP data of Mukherjee *et al.* (2014), but the mooring off Cuddalore in southeast India also shows downward phase propagation in 2010 (Mukherjee *et al.* 2014); such downward phase propagation is also seen on occasions off the Indian west coast (Amol *et al.* 2012, 2014). This upward propagation of phase implies the existence of undercurrents, with the depth of transition moving closer to the surface over time (Mukherjee *et al.* 2014); the undercurrent associated with the EICC is particularly striking off Cuddalore in the south. At the seasonal time scales, the interference of multiple processes, with the equatorward EICC forced by interior Ekman pumping and equatorial forcing opposing the poleward EICC forced by the local alongshore winds, also leads to an undercurrent (Shankar *et al.* 1996; McCreary *et al.* 1996; Vinayachandran *et al.* 1996).

Though the ADCP moorings have enabled quantification of the intraseasonal variability of the EICC, the four years of data used by Mukherjee *et al.* (2014) barely resolved the annual cycle, which lay outside the cone of influence in wavelet analysis. In this paper, we add five more years of data (2013–2018) to describe the variability of the EICC. The longer, nine-year record not only brings

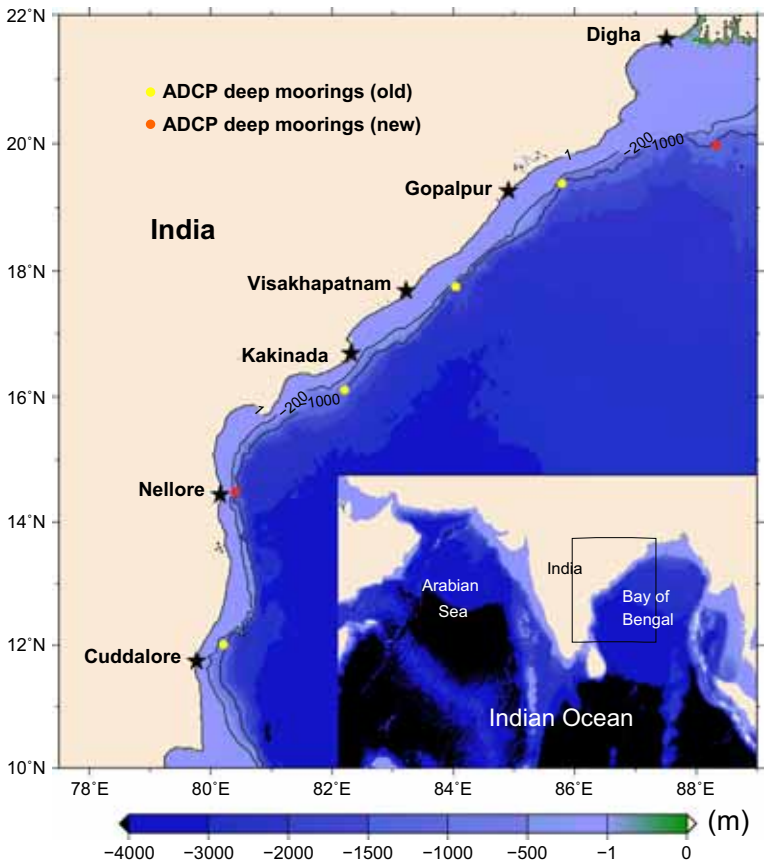

Figure 1. The region of interest, the Bay of Bengal, and its location in the larger region, the north Indian Ocean. The colour scale shows the bathymetry (m). The 200 m (shelf break) and 1000 m contours are overlaid. The solid yellow circles indicate the ADCP locations on the continental slope; the solid red circles indicate the new moorings that have been deployed to augment the mooring network. The black stars on the shore line indicate the closest cities according to which the moorings has been named.

the annual cycle within the cone of influence for several years, but also permits an analysis of variability at sub-annual time scales. The longer data set confirms several of the results of Mukherjee *et al.* (2014), but does so with greater statistical confidence. We also present some new results, particularly for the sub-annual current and the year-to-year modulation of the seasonal and intraseasonal variability. The data sets used are described in section 2. The alongshore and cross-shore components of the sub-inertial EICC are described in section 3, following which the description is restricted largely to the alongshore component. The seasonal cycle of the alongshore EICC is described in section 4 and its intraseasonal and interannual variability are described in section 5. Section 6 discusses the results and concludes the paper.

2. Data and methods

We use data from the ADCP moorings deployed on the continental slope off the Indian east coast; in addition, we use current data from the OSCAR product (Bonjean and Lagerloef 2002). In this section, we describe briefly these two data sets and the methods used to process the ADCP data.

2.1 *ADCP data*

The ADCP data are from four moorings, one each located off Gopalpur (∼19.5°N), Visakhapatnam (∼18°N), Kakinada (∼16°N), and Cuddalore (∼12°N), which are towns on the Indian east coast (figure 1); this nomenclature, with the ADCP moorings being tagged to nearby towns, follows earlier work on the EICC (Mukherjee *et al.* 2013, 2014) and WICC (Amol *et al.* 2014). Of these four locations, data for 2009–2013 from Gopalpur, Kakinada, and Cuddalore were presented by Mukherjee *et al.* (2014). Mukherjee *et al.* (2014) presented data for an additional mooring, which was named 'Paradip': this mooring was deployed in the deeper ocean in the northern bay and is excluded from our analysis. Instead, we have included the mooring off Visakhapatnam, which lies between the moorings off Gopalpur and Kakinada and is therefore more relevant to the EICC. The ADCP and deployment information for the moorings off Gopalpur, Visakhapatnam, Kakinada, and Cuddalore are given in tables 1–4, respectively.

All moorings are deployed on the slope at a depth of ∼1000–1100 m (tables 1–4). For the first few years, the moorings had only one ADCP of frequency 76 kHz and located at ∼300–400 m from the surface. An additional ADCP was added from 2012 onwards. When two or more ADCPs are deployed on the mooring line, the frequency of the top ADCP is 153 kHz and its depth ∼150–200 m. The second ADCP was added to the moorings in a staggered manner and the maximum depth of data availability is therefore not consistent across the four moorings.

All ADCPs used are of make Teledyne RDI. The sampling interval is one hour and the bin size 4 and 8 m for the 153 and 76 kHz ADCPs, respectively. The method used for processing the data largely follows Amol *et al.* (2014) and Mukherjee *et al.* (2014). Tidal components having a period of a day or less are removed using the Tidal Analysis Software Kit (TASK-2000) package of Bell *et al.* (1998) and depth interpolation is carried out following Kutsuwada and McPhaden (2002). Data gaps longer than 12 hrs are filled using the grafting method described in the supplement to Mukhopadhyay *et al.* (2017), who used it to fill short gaps in data from high-frequency (HF) coastal radars. This method uses information from the time series on either side of a gap along with cubic splines to fill the gap sufficiently smooth to ensure that the gap-filling has a weaker impact on the wavelet power spectrum compared to linear interpolation or the use of cubic splines alone. The de-tided currents are then rotated to retrieve the alongshore and sub-inertial cross-shore components: a least-square approach is used to minimise the sub-inertial cross-shore component.

One addition to the procedure used earlier (Amol *et al.* 2014; Mukherjee *et al.* 2014) is a correction for variations in ADCP-transducer depth, which can change with time owing to strong sub-surface flow. This change in depth is indicated by the variation in the pressure measured by a sensor mounted on the transducer. Accounting for this effect shows it has a minor effect, but an exception is seen off Kakinada in February 2013, when the change due to the pressure correction is $\sim 40\,\mathrm{cm\,s^{-1}}$ (figure 2).

The ADCP data are then low-pass-filtered with a 72-hr Lanczos filter to retain only the sub-inertial current. The earlier papers used a fourth-order Butterworth filter, which leads to less loss of

Table 1. *ADCP mooring details for the mooring on the continental slope off* ***Gopalpur****. All the ADCPs deployed were upward-looking and of make Teledyne RDI. The bin size is 8 m (4 m) for the 76 (153) kHz ADCPs. The water depth at the mooring location is ∼1000–1100 m. The angle of rotation, based on the clockwise rotation of the meridional component of the velocity, is 56° for Gopalpur. The columns are as follows. C1: ADCP name; the 'A' in the name represents data from the shallowest (topmost) mooring and 'B' represents the second ADCP in the mooring line. C2: Position (longitude in °E, latitude in °N) and water-column depth (m). C3: Starting and ending dates. C4: Depth of ADCP (m). C5: Frequency, ν (kHz), of the ADCP. C6: Start and end date of the data gap(s); when there are no data gaps for a deployment, this column is left blank.*

ADCP	Position/Depth		Start date	End date	ADCP depth	ν	Data gap
BOGD1	85.44	18.86/1058	21-04-2009	15-05-2010	328	76.8	
BOGD2	85.80	19.38/1027	15-05-2010	21-03-2011	296	76.8	
BOGD3	85.79	19.38/1040	21-03-2011	17-02-2012	295	76.8	
BGD4A	85.79	19.38/1048	16-02-2012	10-10-2012	214	153.6	10-10-2012–20-03-2013
BGD5A	85.79	19.40/1041	20-03-2013	27-02-2014	174	153.6	
BGD5B	85.79	19.40/1041	20-03-2013	27-02-2014	582	76.8	
BGD6A	85.79	19.40/1063	27-02-2014	11-03-2015	198	153.6	
BGD6B	85.79	19.40/1063	27-02-2014	11-03-2015	603	76.8	
BGD7A	85.79	19.39/1113	12-03-2015	01-05-2015	268	153.6	1-05-2015–18-02-2017
BGD7B	85.79	19.39/1113	12-03-2015	20-03-2016	674	76.8	No data up to 236 m
BGD8A	85.79	19.40/1058	20-03-2016	12-04-2016	215	153.6	
BGD8B	85.79	19.40/1058	20-03-2016	18-02-2017	618	76.8	No data up to 192 m
BGD9A	85.79	19.40/1107	18-02-2017	15-04-2018	182	153.6	
BGD9B	85.79	19.40/1107	18-02-2017	15-04-2018	587	76.8	

Table 2. *ADCP mooring details for the mooring on the continental slope off* ***Visakhapatnam****. All the ADCPs deployed were upward-looking and of make Teledyne RDI. The bin size is 8 m (4 m) for the 76 (153) kHz ADCPs. The water depth at the mooring location is ∼1000–1100 m. The angle of rotation, based on the clockwise rotation of the meridional component of the velocity, is 47° for Visakhapatnam. The columns are as follows. C1: ADCP name; the 'A' in the name represents data from the shallowest (topmost) mooring and 'B' represents the second ADCP in the mooring line. C2: Position (longitude in °E, latitude in °N) and water-column depth (m). C3: Starting and ending dates. C4: Depth of ADCP (m). C5: Frequency, ν (kHz), of the ADCP. C6: Start and end date of the data gap(s); when there are no data gaps for a deployment, this column is left blank.*

ADCP	Position/Depth		Start date	End date	ADCP depth	ν	Data gap
BOVD1	84.02	17.74/1081	25-03-2011	15-02-2012	366	76.8	
BVD2A	84.02	17.74/1034	15-02-2012	04-02-2013	161	153.6	
BVD2B	84.02	17.74/1034	15-02-2012	17-03-2013	189	76.8	
BVD3A	84.03	17.75/953	18-03-2013	24-02-2014	100	153.6	04-02-2013–18-03-2013
BVD3B	84.03	17.75/953	18-03-2013	24-02-2014	514	76.8	
BVD4A	84.06	17.75/1013	25-02-2014	09-03-2015	158	153.6	
BVD4B	84.06	17.75/1013	25-02-2014	09-03-2015	572	76.8	
BOVD5	84.06	17.76/953	09-03-2015	18-03-2016	228	76.8	
BOVD6	84.06	17.76/979	18-03-2016	16-02-2017	257	76.8	
BOVD7	84.05	17.75/898	16-02-2017	14-04-2018	176	76.8	

data at the ends of the time series (including the data gaps), but it is more difficult to interpret the filtered currents at such edges in the time series. Though the Lanczos filter leads to more loss of data near the edges, the distortion of the filtered current is much lower. The shorter data sets used by Mukherjee *et al.* (2014) and Amol *et al.* (2014) did not have such data gaps, permitting the use of the Butterworth filter.

In the rest of this paper, the basic data set consists of the sub-inertial, rotated (alongshore and cross-shore) currents estimated from the ADCP data.

2.2 *OSCAR*

The OSCAR product provides an estimate of the near-surface current averaged over the top ∼30 m. The data are provided at an interval of five days on a

Table 3. *ADCP mooring details for the mooring on the continental slope off* ***Kakinada****. All the ADCPs deployed were upward-looking and of make Teledyne RDI. The bin size is 8 m (4 m) for the 76 (153) kHz ADCPs. The water depth at the mooring location is ∼1000–1100 m. The angle of rotation, based on the clockwise rotation of the meridional component of the velocity, is 42° for Kakinada. The columns are as follows. C1: ADCP name; the 'A' in the name represents data from the shallowest (topmost) mooring and 'B' represents the second ADCP in the mooring line. C2: Position (longitude in °E, latitude in °N) and water-column depth (m). C3: Starting and ending dates. C4: Depth of ADCP (m). C5: Frequency, ν (kHz), of the ADCP. C6: Start and end date of the data gap(s); when there are no data gaps for a deployment, this column is left blank.*

ADCP	Position/Depth		Start date	End date	ADCP depth	ν	Data gap
BVKD1	82.98	16.84/1073	20-04-2009	14-05-2010	365	76.8	
BOKD1	82.50	16.39/1003	11-05-2010	27-03-2011	265	76.8	
BOKD2	82.52	16.40/1065	27-03-2011	12-02-2012	277	76.8	
BOKD3	82.61	16.45/1048	13-02-2012	15-03-2013	343	76.8	
BOKD4	82.18	16.05/1063	15-05-2013	23-02-2014	311	76.8	
BOKD5	82.21	16.10/890	23-02-2014	07-03-2015	238	76.8	
BKD6A	82.20	16.10/908	07-03-2015	no data	340	153.6	
BKD6B	82.21	16.10/908	07-03-2015	16-03-2016	475	76.8	
BKD7A	82.22	16.13/912	16-03-2016	21-03-2016	400	153.6	
BKD7B	82.22	16.13/912	16-03-2016	14-02-2017	478	76.8	14-02-2017–10-03-2017
BKD8A	82.22	16.13/918	10-03-2017	24-04-2018	185	153.6	
BKD8B	82.22	16.13/918	14-02-2017	24-04-2018	292	76.8	

Table 4. *ADCP mooring details for the mooring on the continental slope off* ***Cuddalore****. All the ADCPs deployed were upward-looking and of make Teledyne RDI. The bin size is 8 m (4 m) for the 76 (153) kHz ADCPs. The water depth at the mooring location is ∼ 1000–1100 m. The angle of rotation, based on the clockwise rotation of the meridional component of the velocity, is 30° for Cuddalore. The columns are as follows. C1: ADCP name; the 'A' in the name represents data from the shallowest (topmost) mooring and 'B' represents the second ADCP in the mooring line. C2: Position (longitude in °E, latitude in °N) and water-column depth (m). C3: Starting and ending dates. C4: Depth of ADCP (m). C5: Frequency, ν (kHz), of the ADCP. C6: Start and end date of the data gap(s); when there are no data gaps for a deployment, this column is left blank.*

ADCP	Position/Depth		Start date	End date	ADCP depth	ν	Data gap
BOPD1	80.20	12.02/1087	26-03-2010	02-05-2011	427	76.8	
BOPD2	80.20	12.02/1088	02-05-2011	10-02-2012	321	76.8	
BOPD3	80.21	12.02/1089	10-02-2012	12-03-2013	325	76.8	
BPD4A	80.20	12.01/1124	12-03-2013	20-02-2014	187	153.6	
BPD4B	80.20	12.01/1124	12-03-2013	20-02-2014	692	76.8	
BPD5A	80.20	12.01/1111	21-02-2014	04-03-2015	174	153.6	
BPD5B	80.20	12.01/1111	21-02-2014	04-03-2015	679	76.8	
BPD6A	80.21	12.01/975	04-03-2015	14-03-2016	37	153.6	
BPD6B	80.20	12.00/975	04-03-2015	14-03-2016	462	76.8	
BPD7A	80.21	12.02/1239	14-03-2016	24-01-2017	292	153.6	14-03-2016–12-02-2017 (No data up to 96 m)
BPD8A	80.21	12.01/1166	12-02-2017	27-04-2018	223	153.6	
BPD8B	80.21	12.01/1166	12-02-2017	27-04-2018	654	76.8	24-01-2017–12-02-2017

global grid and are freely available from 1992 onwards (Bonjean and Lagerloef 2002) at the websites of both NOAA (National Oceanic and Atmospheric Administration) and NASA (National Aeronautics and Space Administration). The NASA site, http://podaac.jpl.nasa.gov/, serves OSCAR data at two resolutions, $1^\circ \times 1^\circ$ and $0.33^\circ \times 0.33^\circ$; we use the fine-resolution data in this paper.

A comparison for the alongshore component shows that the OSCAR current matches the ADCP current well (figure 3). The wavelet coherence is high throughout the time series at periods exceeding ∼100 days, i.e., for the seasonal cycle (figure 4). A similar result was obtained by Mukherjee *et al.* (2014) for the shorter ADCP data set. There are however, differences between the two data sets and they show up primarily in the phase, with the OSCAR current usually tending to lag the ADCP current, but there are occasions when it leads the ADCP current.

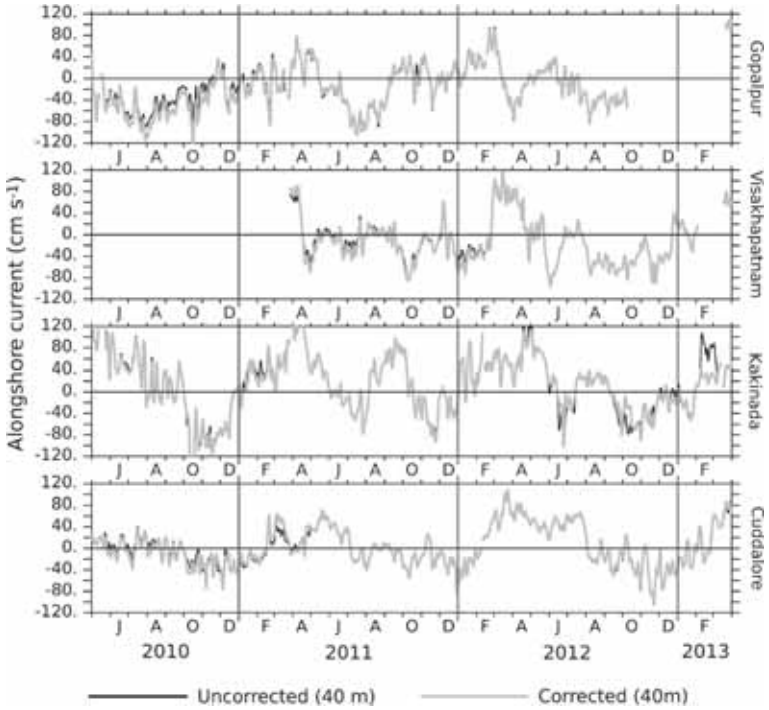

Figure 2. Alongshore currents ($\mathrm{cm\,s^{-1}}$) at all four mooring locations during 2009–2013 before (black) and after (grey) the pressure correction (section 2.1). The change is shown for the period covered in Mukherjee *et al.* (2014).

3. The sub-inertial EICC

Since the top (bottom) ADCP bin for which data are available throughout the time series at all locations is at 48 m (200 m), most of the analysis is restricted to the top 200 m. We do, however, present the sub-inertial currents up to 300 m because the loss due to filtering is much less than for the longer filters used for the intraseasonal or seasonal currents. Likewise, whenever a 153 kHz ADCP was available at depths shallower than ∼350 m, the sub-inertial current is available closer to the surface up to ∼24 m. The sub-inertial alongshore and cross-shore components are discussed in this section. We divide the year into three seasons for convenience and consistency with the literature: spring (often called 'spring inter-monsoon') refers to February–April, summer or summer monsoon to June–August, and winter or winter monsoon to October–December, with January, May, and September representing the transition between seasons.

3.1 *Alongshore component*

The seasonality of the alongshore EICC – strong poleward flow during spring and equatorward flow during winter – is apparent at all four locations in the longer data set (figure 5), confirming that these canonical directions attributed to the EICC in the literature (Shetye *et al.* 1991, 1993, 1996; McCreary *et al.* 1993, 1996) are robust features of its seasonal cycle and therefore show up clearly in climatologies (Cutler and Swallow 1984; Mariano *et al.* 1995).

During the summer monsoon, when the direction of the EICC is less clear owing to the opposing currents forced by local and remote winds (McCreary *et al.* 1993, 1996; Shankar *et al.* 1996, 2002; Vinayachandran *et al.* 1996), the expected equatorward flow is seen near the northern end of the coast off Gopalpur in the years for which data are available, but the expected weak, poleward, near-surface flow at other locations is not evident in all years. At Cuddalore, for example, the EICC flows equatorward at 48 m during the summer monsoons of 2010, 2013, 2014, and 2017, and poleward flow is restricted to the summer monsoons of 2012 and 2015; data are not available in 2016 above 96 m (table 4) and there is a weak poleward burst early during the summer monsoon of 2011. Even off Visakhapatnam and Kakinada, the flow is poleward only in a few years.

The vertical extent of the EICC varies along the coast. Off Gopalpur, the current decays with depth and an undercurrent is evident on occasions. The undercurrent, as noted earlier by Mukherjee *et al.* (2014), is

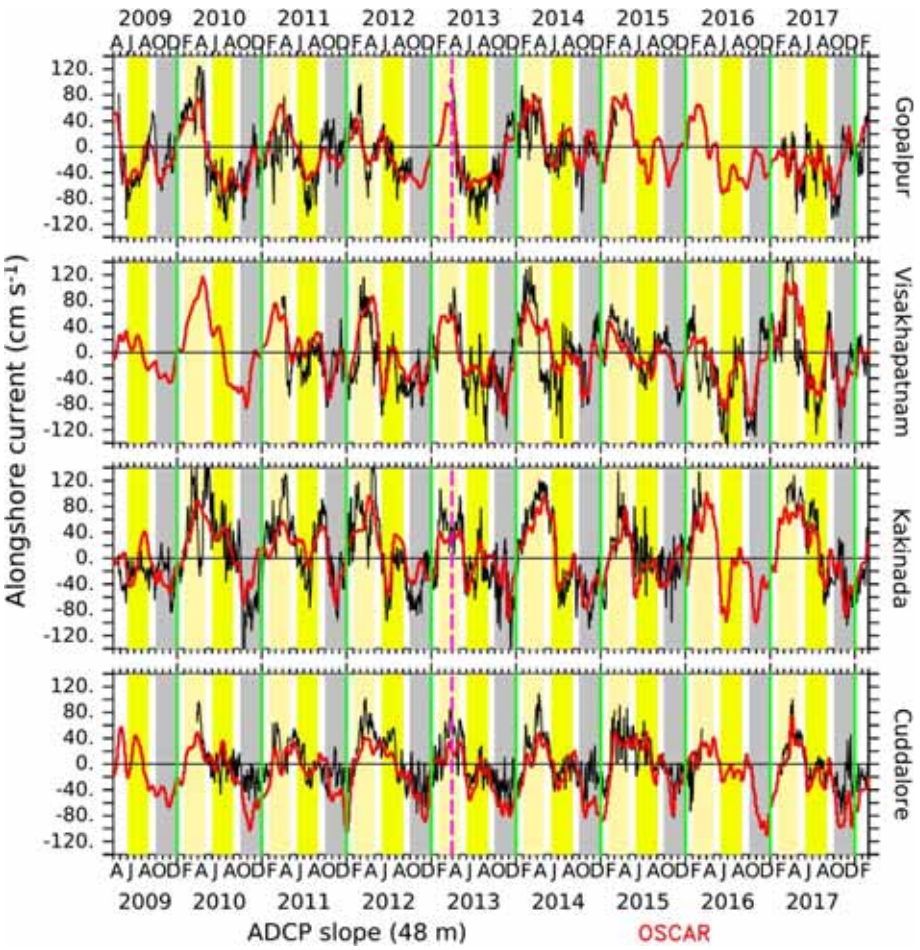

Figure 3. The sub-inertial alongshore current ($\mathrm{cm\,s^{-1}}$) at all four mooring locations estimated from the ADCP (black curves) and OSCAR (red curves) data; the ADCP current is at 48 m and the OSCAR current represents an average over the top ∼30 m. Poleward (equatorward) currents are positive (negative) and the OSCAR grid point nearest to the ADCP mooring location has been used for the comparison. The beige, yellow, and grey shading represents spring (February–April), summer monsoon (June–August), and winter monsoon (October–December), respectively, with May, September, and January marking the transition between these seasons. The green vertical lines are used to separate the years and the dashed magenta vertical lines mark the end of the period for which Mukherjee *et al.* (2014) presented the data; they did not present the data for Visakhapatnam.

more prominent off Cuddalore, where it is seen in most years. The alongshore EICC is a deep current only off Visakhapatnam and Kakinada, particularly the former location. Note the near merger of the curves for 48, 104, and 200 m off Visakhapatnam when the transition occurs from the strong poleward flow during spring to the often equatorward flow during the summer monsoon; a similar transition is often seen from summer to winter as well, marking a reversal in direction over a significant depth range.

The EICC off Visakhapatnam, for which data were not presented by Mukherjee *et al.* (2014), shows significant differences from both Gopalpur to its north and Kakinada to its south even though the separation is ∼200 km. The duration of the poleward flow during spring is different and so is the EICC direction on several occasions, an example of which is seen during December 2014, when the EICC flows equatorward off Gopalpur and Kakinada, but is poleward off Visakhapatnam. This change in direction suggests a decorrelation of the alongshore EICC, which has been noted earlier for intraseasonal time scales (Durand *et al.* 2009; Mukherjee *et al.* 2014).

Wavelet analysis shows a strong seasonal cycle at all four locations, including Visakhapatnam (figure 6). Following Mukherjee *et al.* (2014), we split the seasonal cycle into an annual cycle, which has a period around ∼365 days, and intra-annual variability, which consists of the semi-annual cycle (period ∼180 days) and a band around 120 days. Notwithstanding the data gaps, the longer data record leads to the annual cycle lying within the

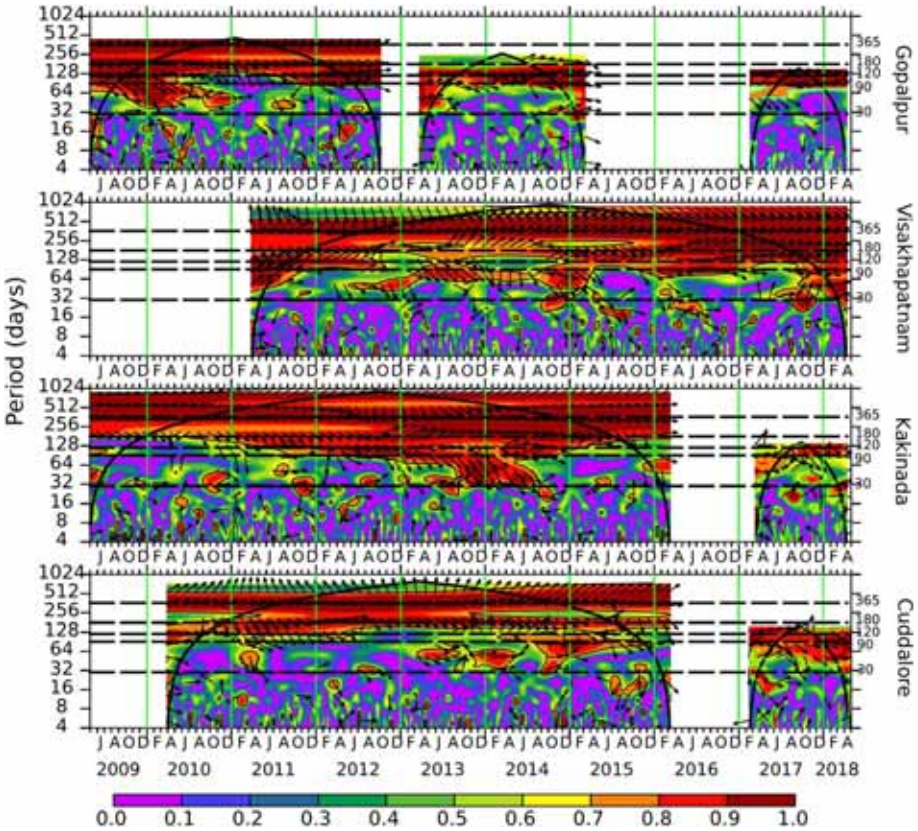

Figure 4. The wavelet coherence between the ADCP (48 m) and OSCAR current; the ordinate for these panels is the period (days) plotted on a $\log_2$ scale. The thick black curve marks the cone of influence and the coherence above the 95% significance level is marked by the black contours. The phase difference is shown by the arrows, which are marked only if the coherence exceeds 0.5. The ADCP current leads (lags) the OSCAR current in anticlockwise (clockwise) direction. The horizontal dashed lines mark 365, 180, 120, 90, and 30 days on the ordinate. In all four panels, the vertical green lines are used to separate the years.

cone of influence of the wavelet off Visakhapatnam, Kakinada, and Cuddalore; even off Gopalpur, where two large gaps split the wavelet spectrum into three time slices, the wavelet power for 2010–2011 falls within the cone of influence, implying that it is statistically reliable. The annual cycle is strong at all four locations and it yields the highest peak in an FFT (Fast Fourier Transform) analysis (figure 7), but, as we shall see in section 4.2, the dominant component in the intra-annual band switches between the semi-annual and 120-day bands in different years.

3.2 *Cross-shore component*

As noted by Mukherjee *et al.* (2014) for 2009–2013, the cross-shore component of the EICC during 2013–2018 also is much weaker (figure 8) than its alongshore component (figure 5).

Strong cross-shore flow, with rapid changes in direction, is seen off Gopalpur during spring in 2011 and 2014, both years with strong, long-lived poleward flow. Strong inshore flow, associated with strong equatorward flow, is seen during the summer monsoons of 2010 and 2013.

Offshore flow is strong, with magnitude exceeding $30\,\mathrm{cm\,s^{-1}}$, during spring 2012 and 2017 off Visakhapatnam. The poleward flow is also stronger during spring in these years, but the comparable poleward flow during spring 2014 is not associated with a strong cross-shore flow. Strong inshore flows are of much shorter duration and occur usually during May.

The strongest cross-shore flow is seen off Kakinada, where offshore flow is strong during April 2011, February and April 2012, May 2013, March–April and June 2014, and June–July 2017. On all these occasions, the offshore flow (figure 8) is associated with a strong poleward flow (figure 5), but there are several occasions when comparable poleward flow occurs without a strong cross-shore counterpart. Inshore flow is generally weaker, but there are strong bursts during winter in 2013 and 2014 and during May–December 2015. The

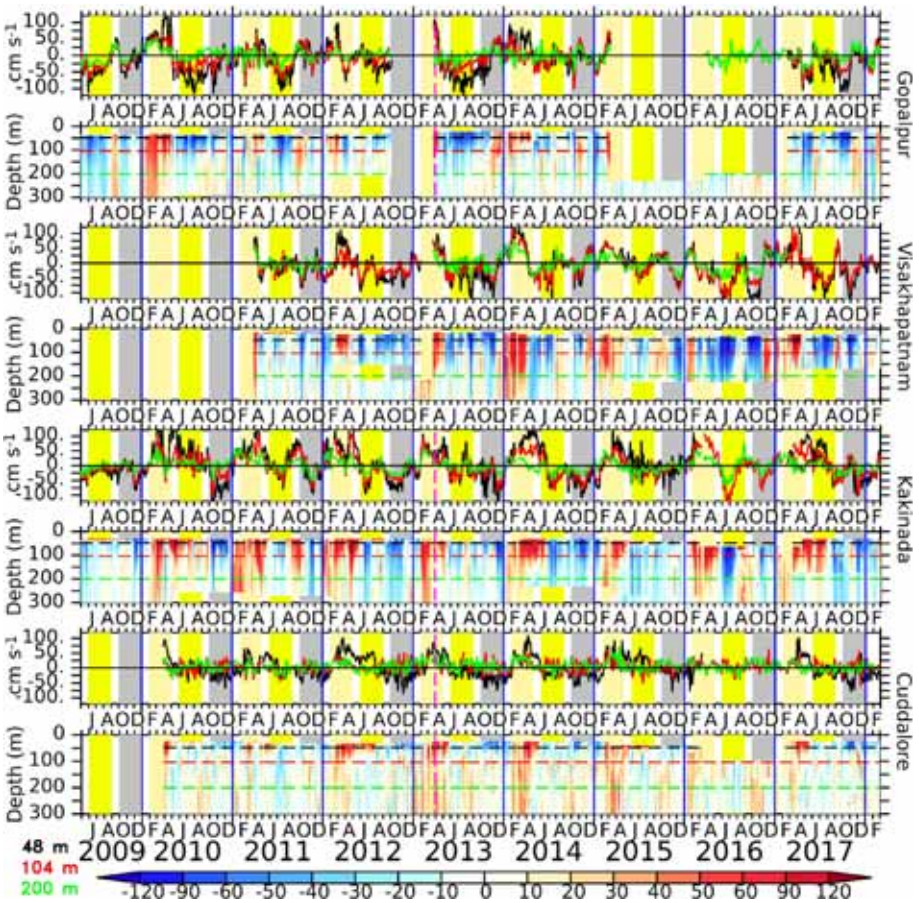

Figure 5. The sub-inertial alongshore current ($\mathrm{cm\,s^{-1}}$) at all four mooring locations. A poleward current is positive. The odd panels show the current at 48 m (black), 104 m (red), and 200 m (green) and the even panels show the depth-time variation of the sub-inertial current, with the same colours used to mark these depths. The beige, yellow, and grey shading represents spring (February–April), summer monsoon (June–August), and winter monsoon (October–December), respectively, with May, September, and January marking the transition between these seasons. The dashed magenta vertical line (during 2013) in the odd panels marks the end of the period for which Mukherjee *et al.* (2014) presented the data; they did not present the data for Visakhapatnam. Note that the colour scale is not uniform in the even panels. In all eight panels, the vertical blue lines are used to separate the years.

association of inshore flow with the alongshore component is not as striking because the equatorward flow is strong not only during winter 2013 and 2014, but also in other years, and the alongshore component is not strong during 2015.

Cross-shore flow is generally weak off Cuddalore, but strong offshore bursts occur during November 2012 and January–February 2016. Both occurrences are associated with strong equatorward flow. Comparable equatorward flow in other years is not, however, associated with a comparable cross-shore component. Inshore flow is strong in during April–May 2015 and April 2017 and is associated with strong poleward flow on both occasions, but comparable poleward flow in some other years is not associated with a comparable cross-shore current.

In summary, strong cross-shore flow in the EICC regime tends to be associated with strong alongshore flows, but the converse is not true: a strong alongshore flow does not guarantee a strong cross-shore flow.

4. The seasonal cycle of the EICC

As noted earlier, the seasonal cycle consists of the annual cycle and intra-annual variability consisting of the semi-annual and 120-day bands. In this section, we filter the alongshore current with band-pass Lanczos filters to quantify the variability in the annual (300–400 days band-pass-filtered) and intra-annual (100–250 days band-pass-filtered) bands. The Lanczos filter involves weights. Increasing the number of weights increases the

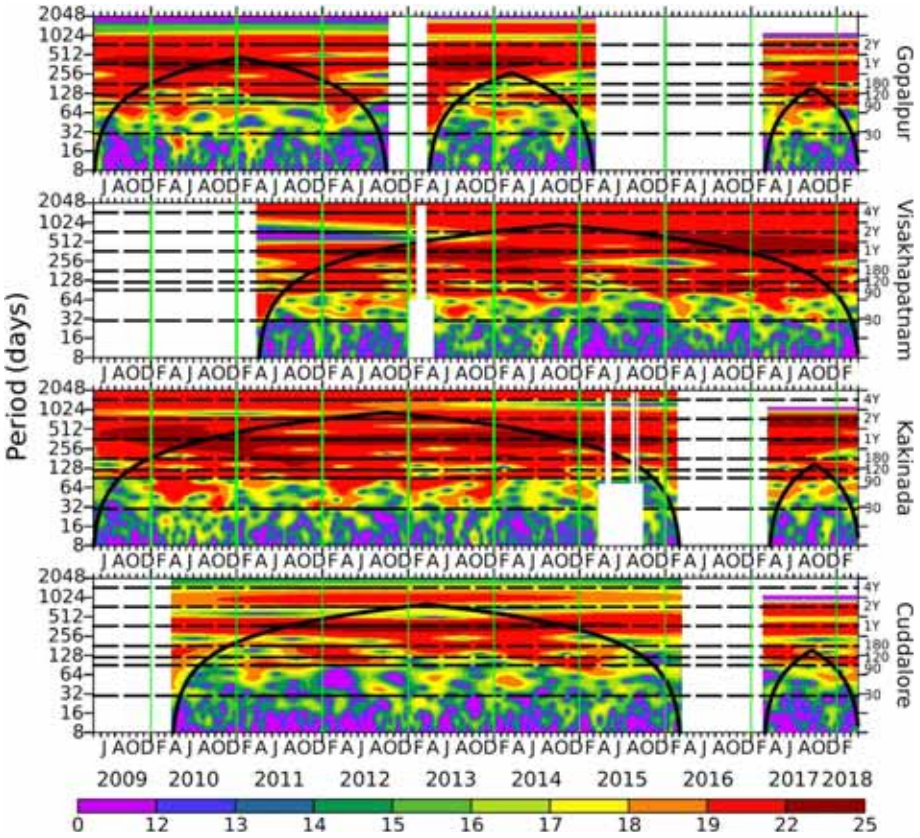

Figure 6. Morlet wavelet power spectrum ($cm^2\ s^{-2}$) for the alongshore ADCP current at 48 m at all four mooring locations. The ordinate is the period (days) plotted on a $\log_2$ scale; a $\log_2$ scale is also used for the wavelet power, for which the colour scale is not uniform. The thick black curve represents the cone of influence. The horizontal lines mark 4, 2, and 1 yr or 365 days (annual band), 180 days (semi-annual band), 120 days, 90 days, and 30 days. The semi-annual and 120-day bands constitute the intra-annual variability and the low-frequency (high-frequency) part of the intraseasonal variability is contained in the 30–90-day band (4–30-day band).

response in the center of the frequency band being considered and this number increases inversely with the difference $f_1 - f_2$, where f_1 and f_2 ($f_1 > f_2$) are the two cut-off frequencies for the band. However, increasing the number of weights also increases the loss of data near gap edges or at the ends of the time series. Therefore, the choice of weights is a compromise between getting an accurate estimate of the signal in the band and the loss of data. While this loss of data does not matter for the intraseasonal and even the intra-annual bands, it does matter for the annual band. Therefore, while the weighting window is $3/f_2$, where f_2 is the lower frequency (in the units of the time interval used for the analysis), for the intra-annual and lower periods, we use $1.5/f_2$ for the annual band.

4.1 *The annual cycle*

In the FFT (figure 7) and wavelet (figure 6) spectra, the annual cycle dominates the seasonal variability at all four locations, but its magnitude varies over the time series (figure 6). Though this interannual modulation of the annual cycle is more clear off Visakhapatnam and Kakinada in the filtered current and a depth-time plot of the wavelet power extracted around the annual band owing to the longer continuous data record at these locations, it is also evident off Gopalpur and Cuddalore (figure 9). Off Kakinada, the magnitude of the annual current increases by ∼30–35% from 2010 to a peak in 2014; following a decrease from this peak in 2015, it increases again in 2016. Off Visakhapatnam too, the magnitude increases by ∼40% from 2012 to 2013–2014; following a decrease of ∼60% from 2014 to 2015, the magnitude increases again in 2016–2017. Off Gopalpur, the annual cycle seems to peak in 2010 and again in 2013; data gaps preclude a more complete analysis, but the data suggest lower magnitudes between 2010–2013 and from mid-2014 onwards. Off Cuddalore, as noted earlier, the strong annual cycle is shallower, with

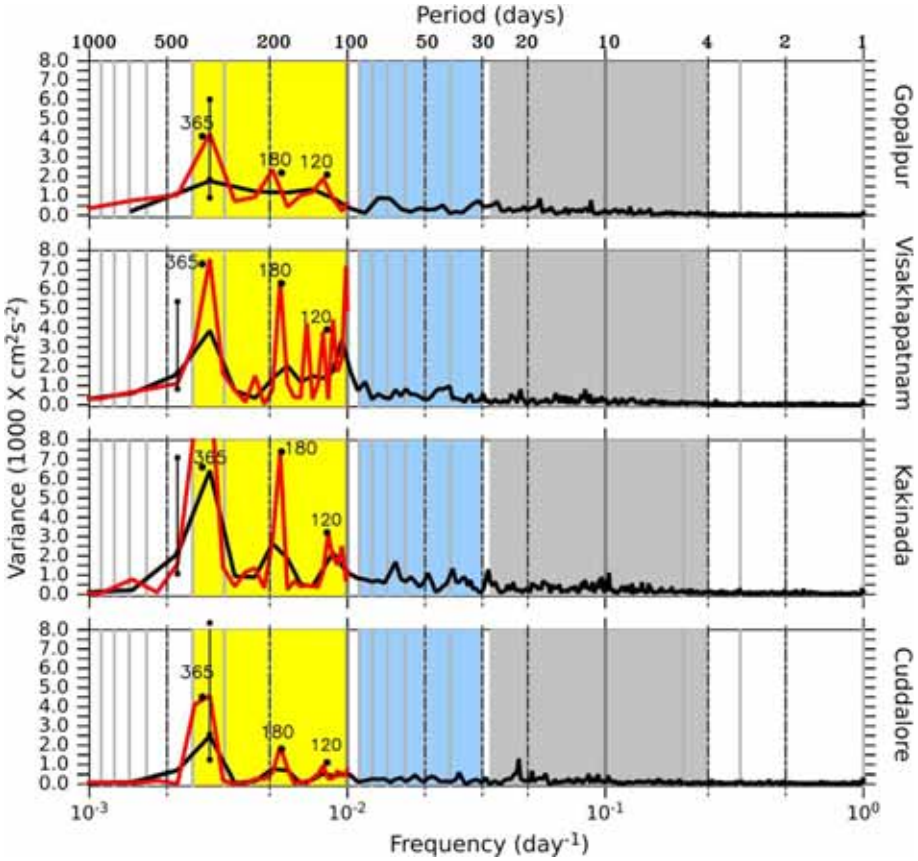

Figure 7. Variance-preserving spectra (black curves; $10^3\,\mathrm{cm^2\,s^{-2}}$) for the raw alongshore currents at 48 m. The abssica is the frequency ($\mathrm{days^{-1}}$) plotted on a $\log_2$ scale. The Fast Fourier Transform (FFT) was carried out for different durations owing to the data gaps. The panel for Gopalpur (top) shows the FFT over 2009–2013, that for Visakhapatnam (second panel) over 2011–2018, for Kakinada panel (third panel) over 2009–2016, and that for Cuddalore (bottom panel) over 2010–2016. As done by Mukherjee *et al.* (2014), the spectra were smoothed using a three-point triangle filter after applying a 75% Tukey window to the detrended and detided data. The bar in the lower left corner of all panels represents the 95% confidence interval. The yellow, light blue, and grey shades highlight the seasonal cycle (100–400 days) and the intraseasonal (30–90 days) and high-frequency (4–25 days) bands, respectively. The dashed red curves show the raw spectra (not smoothed) for the seasonal band. The period for major peaks is listed.

the peak occurring in 2013. At all locations, an increase in the magnitude of the annual cycle is associated with an increase in the depth range: this association can be seen by following a contour for the wavelet power in the wavelet panels of figure 9. The depth up to which the annual cycle is strong does, however, change with location, increasing from the northern bay to the central bay before decreasing again farther south.

Upward phase propagation is evident at all four locations, but the phase speed appears to be higher (isolines of phase more vertical) off Visakhapatnam compared to other three locations. The wavelet coherence between the ADCP current at 48 m and the OSCAR current, which represents an average over the top $\sim$30 m, is high for the annual cycle throughout the record, but the ADCP current leads the OSCAR current (figure 4), which suggests upward propagation of phase even above 48 m. The minimum difference in phase occurs off Kakinada, where the ADCP and OSCAR current tend to be in phase over most of the record. The longer data record brings much of the annual band within the cone of influence (figure 6), making these coherences statistically significant.

Notwithstanding the alongshore, or inter-moorings, differences in the annual cycle, the ADCP data show that it is highly coherent along the coast (figure 10), a conclusion reached earlier by Durand *et al.* (2009) on the basis of along-track altimeter data and Mukherjee *et al.* (2014) on the basis of ADCP data. As noted by Mukherjee *et al.* (2014), the phase changes along the coast, with the northern location tending to lead the southern location. Accordingly, the current off Visakhapatnam (Kakinada) leads that off Kakinada

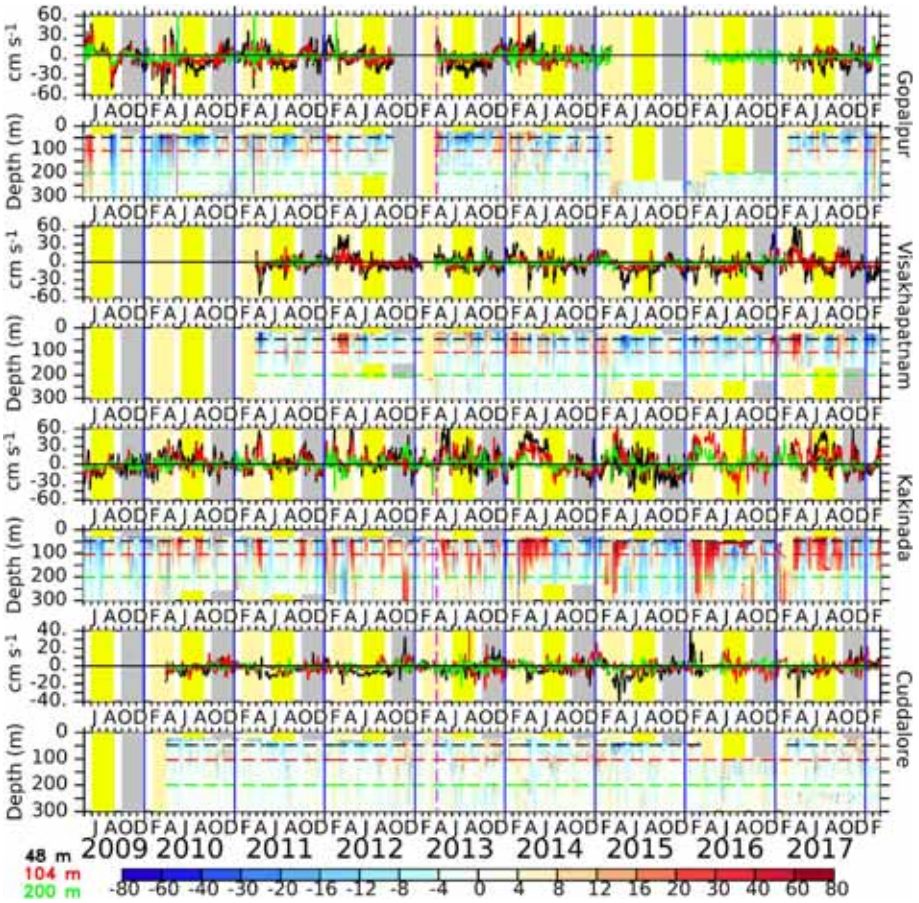

Figure 8. The sub-inertial cross-shore current ($cm\,s^{-1}$) at all four mooring locations. Offshore or upwelling-favourable flow is positive. The odd panels show the current at 48 m (black), 104 m (red), and 200 m (green) and the even panels show the depth-time variation of the sub-inertial current, with the same colours used to mark these depths. The beige, yellow, and grey shading represents spring (February–April), summer monsoon (June–August), and winter monsoon (October–December), respectively, with May, September, and January marking the transition between these seasons. The dashed magenta vertical line (during 2013) in the odd panels marks the end of the period for which Mukherjee *et al.* (2014) presented the data; they did not present the data for Visakhapatnam. Note that the colour scale is not uniform in the even panels. In all eight panels, the vertical blue lines are used to separate the years.

(Cuddalore); a similar pattern is seen between Gopalpur and Kakinada, but the annual band lies outside the cone of influence owing to the data gaps off Gopalpur.

4.2 *Intra-annual variability*

Mukherjee *et al.* (2014) noted that the intra-annual variability shows a dominance of the semi-annual or 120-day cycles at different locations in different years and seasons. The 120-day band is most clearly seen off Visakhapatnam in 2016, when the wavelet power (figure 6) is higher in the 120-day band compared to the semi-annual band. The two bands are usually merged in most years, making it difficult to distinguish them as distinct bands, but the distinction between them becomes apparent in years when the 120-day variability is weak: off Visakhapatnam, examples are during mid-2013 to mid-2014 and again in 2015 (figure 6). When the 120-day band is strong, the number of current reversals in a year exceeds four (figure 11), which is the expected number for the semi-annual band. Examples of a strong 120-day band include 2012 and 2016 off Visakhapatnam (figures 6, 11). Off Kakinada, the 120-day variability is striking during 2015, when the number of current reversals exceeds four (figure 11), but the loss of data in the top few bins leads to a gap in the wavelet spectrum (figure 6). In other years like 2011, 2012, and 2014, the 120-day variability captured in the wavelet spectrum (figure 6) appears in the band-passed data (figure 11) as a modulation of the semi-annual cycle above $\sim$150 m, with the poleward EICC weakening between two stronger peaks during January–May. Below $\sim$150 m, however, the EICC

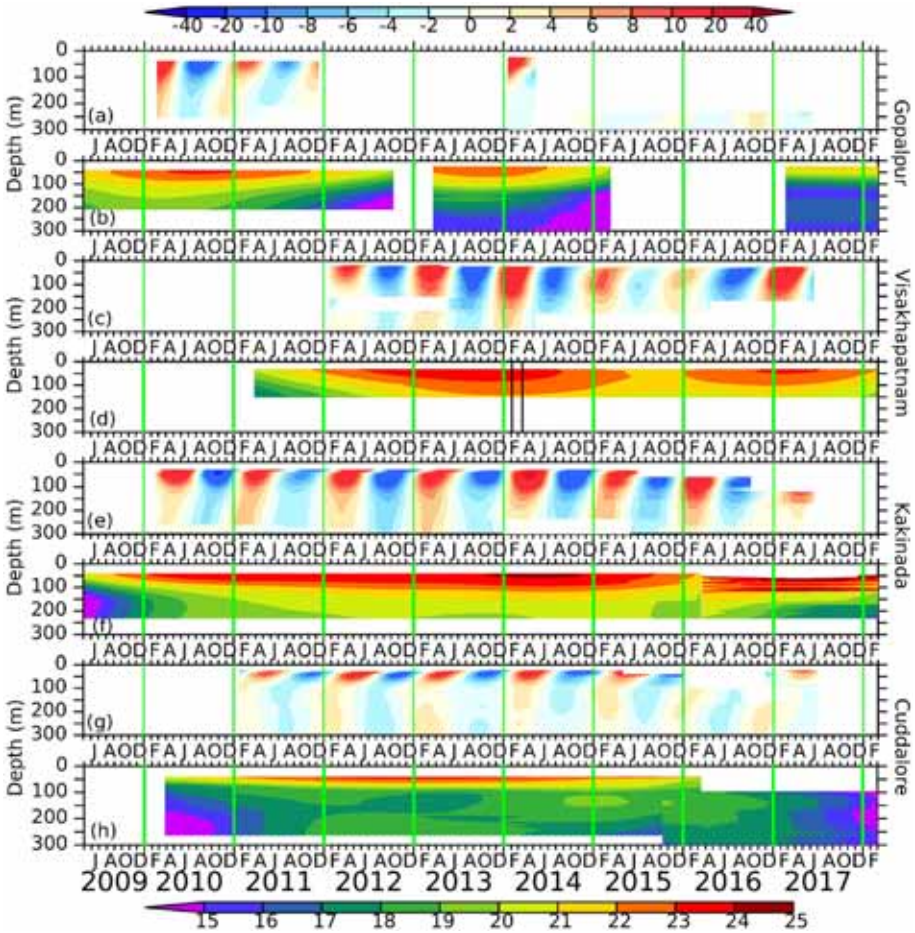

Figure 9. The annual cycle of the alongshore current. The odd panels show the annual cycle (cm s^{-1}), estimated using a 300–400-day Lanczos filter, as a function of time (abscissa) and depth (m, ordinate). Poleward (equatorward) flow is red (blue). The non-uniform colour key for the odd panels is shown at the top. The even panels show the band-averaged annual wavelet power (cm^2 s^{-2}, plotted on a $\log_2$ scale) as a function of time and depth; the colour scale is at the bottom. The vertical black lines in the wavelet panel for Visakhapatnam (during 2014) mark the gap that was filled using the grafting method described in the supplement of Mukhopadhyay *et al.* (2017). In all eight panels, the vertical green lines are used to separate the years.

actually reverses at the time of the weakening of the near-surface EICC. Though the data set off Gopalpur is limited, this switching within the intra-annual band is seen there as well. It is only off Cuddalore that the semi-annual band is stronger than the 120-day band throughout, but the 120-day band is strong in patches, with peaks in 2012, 2014, and 2017 (figure 6).

Though the wavelet spectrum shows a higher power (figure 6) and the FFT a higher peak (figure 7) for the annual cycle compared to the intra-annual bands, the filtered currents show that the intra-annual component (figure 11) is stronger than the annual cycle (figure 9). This difference arises because the wavelet analysis used here follows Torrence and Compo (1998), whose method leads to a flat white-noise spectrum, but, as noted by Maraun and Kurths (2004), a consequence is that sine functions of equal amplitude exhibit different integrated powers proportional to their oscillation scale. As a results, it is not possible to compare the variability across period bands, but it is possible to compare variability within a specific band over the time series (Chaudhuri *et al.* 2020). Hence, though the wavelet analysis suggests a stronger annual cycle, the intra-annual component tends to be stronger, but both annual and intra-annual components vary over the time series (figures 9, 11).

Phase propagates upward in the intra-annual band off Gopalpur, Visakhapatnam, and Kakinada (figure 11). Off Cuddalore, however, downward propagation of phase, noted by Mukherjee *et al.* (2014) during winter 2010, is common during the summer and winter monsoons. This downward propagation of phase, which is limited to the top

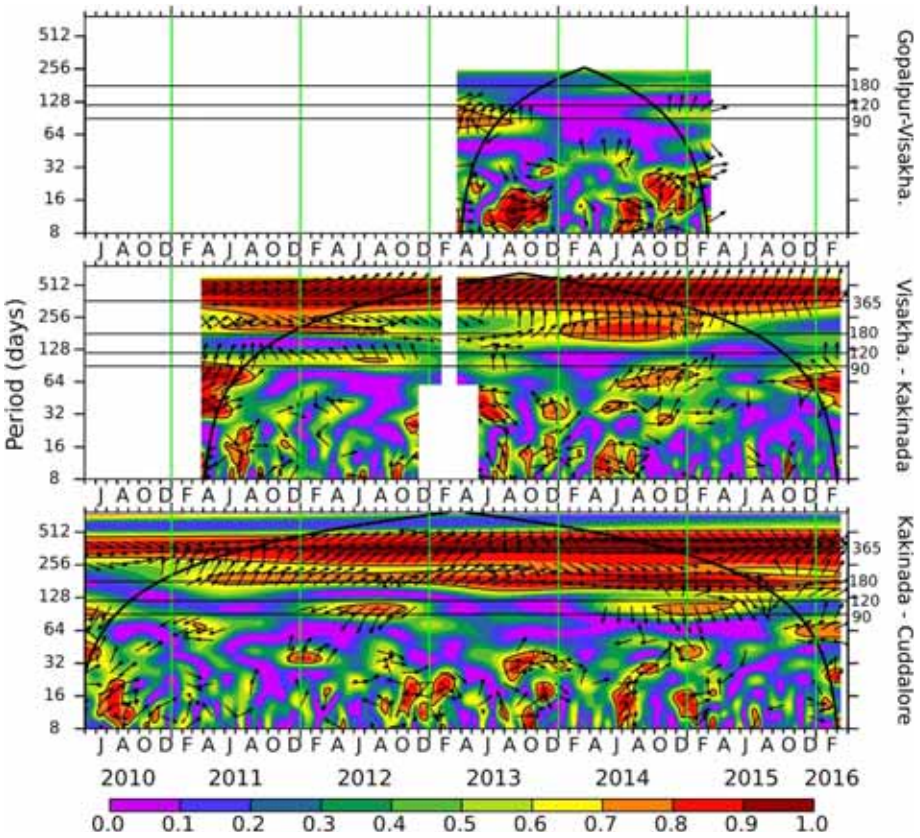

Figure 10. Alongshore wavelet coherence of the alongshore current at 48 m. The thick black curve represents the cone of influence and the coherence above the 95% significance level is marked by the black contour. The ordinate (period, days) is plotted on a $\log_2$ scale. The horizontal lines mark 365, 180, 120, and 90 days. The top panel shows the coherence between Gopalpur and Visakhapatnam, the middle panel between Visakhapatnam and Kakinada, and the bottom panel between Kakinada and Cuddalore. The phase difference is shown by the arrows, which are marked only if the coherence exceeds 0.5. The current at the northern location leads (lags) the current at the southern in anticlockwise (clockwise) direction.

$\sim$120 m, suggests a combination of local and remote forcing. During spring, however, the phase propagates upward even off Cuddalore, suggesting the dominance of just remote forcing, with the most important mechanism during this transition period of weak winds being the Ekman pumping over the bay (McCreary *et al.* 1993, 1996; Shankar *et al.* 1996, 2002).

A consequence of the switch between semi-annual and 120-day variability within the intra-annual band leads to a variable lead-lag relationship between the ADCP current at 48 m and the OSCAR current (figure 4). Off Cuddalore, since the downward propagation of phase is fairly consistent over the top $\sim$120 m, the ADCP current at 48 m tends to lag the OSCAR current. The distinction, noted earlier between spring and summer or winter, does not, however, show up in the ADCP-OSCAR coherence.

Within the intra-annual band, the alongshore coherence is highest for the semi-annual band between Kakinada and Cuddalore (figure 10). The coherence and the phase do vary over the time series, with Kakinada leading (lagging) Cuddalore before (after) 2013, but the coherence is significant at the 99% level. Between Visakhapatnam and Kakinada, the coherence in the semi-annual band is high only during 2014 (figure 10), when the variability in this band peaks at both locations (figure 6). In contrast, the inter-mooring differences in the variability in the 120-day band (figures 6, 11), which implies an alongshore variation in the 120-day variability, leads to a weaker alongshore coherence for this band (figure 10).

5. Intraseasonal and interannual variability of the EICC

Deviations from the seasonal cycle occur due to variability at intraseasonal and interannual periods, which we quantify in this section.

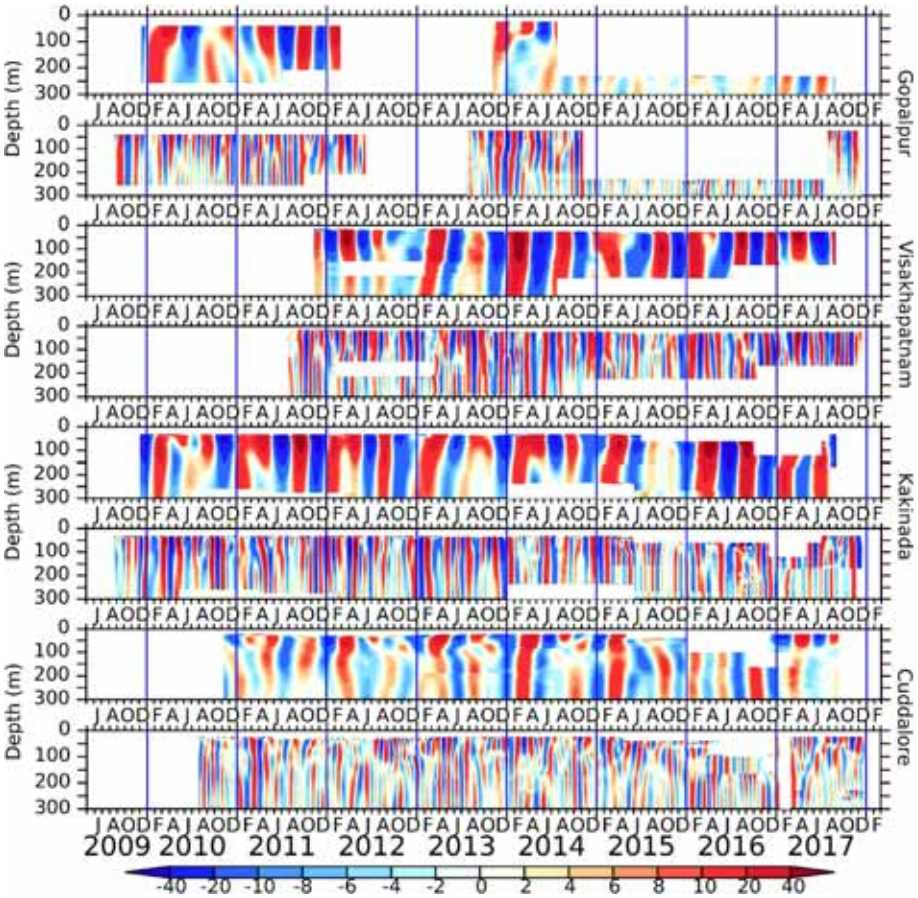

Figure 11. Intra-annual (odd panels) and intraseasonal variability of the alongshore current (cm s^{-1}) at all four locations as a function of time (abscissa) and depth (ordinate, m). A 100–250-day (30–90-day) band-pass Lanczos filter was used to isolate the intra-annual (intraseasonal) periodicities. Note that the colour scale is not uniform. In all eight panels, the vertical blue lines are used to separate the years.

5.1 *Intraseasonal variability*

Following Mukherjee *et al.* (2014), we split the intraseasonal band, which covers the period range from ∼5–100 days, into two bands, with the lower frequencies covering the more traditional 30–90-day band associated with the Madden–Julian Oscillation (MJO; Madden and Julian 1971, 1972), whose signatures have been noted in the altimeter and ADCP data along the Indian coasts (Vialard *et al.* 2009; Suresh *et al.* 2013; Amol *et al.* 2014; Mukherjee *et al.* 2014, 2018). The high-frequency band covers the period range 4–30 days. Intraseasonal variability is strong at all four locations, but, as noted by Mukherjee *et al.* (2014) in the shorter ADCP record, it is weaker than the annual cycle in the wavelet spectrum (figure 6) and the FFT (figure 7). The filtered intraseasonal current (figure 11) is, however, stronger than the annual current (figure 9). Furthermore, the variability in the intraseasonal bands changes with year (figures 6, 11).

Variability in the 30–90-day band is strong at all four locations, but is strongest off Visakhapatnam and Kakinada, suggesting that it is weaker at the northern and southern ends of the Indian east coast (figures 6, 11). The alongshore coherence is, however, weak and patchy (figure 10) in this band and the EICC decorrelates alongshore (Durand *et al.* 2009; Mukherjee *et al.* 2014). For example, the strong variability off Kakinada during 2012 and 2013 is not matched by similar variability off both Visakhapatnam and Cuddalore (figure 6). The variability in this band, as noted by Mukherjee *et al.* (2014), tends to be seasonal, but it peaks in spring only off Cuddalore. Off Gopalpur, the variability in this band peaks during winter in addition to spring; off Visakhapatnam and Kakinada, the peak occurs in different seasons in different years. Off Kakinada, averaging the wavelet power over the 30–90-day band suggests that the variability peaks in spring (figure not shown), as suggested by Mukherjee *et al.* (2014) for the entire EICC regime, but this inference is misleading because the wavelet

power spectrum (figure 6) suggests that the variability at higher periods in this 30–90-day band (i.e., closer to 90 days) is linked to the 120-day variability, while the variability at the shorter periods near 30 days is delinked from the higher periods. Like the intra-annual EICC, the intraseasonal EICC tends to be a deep current, the exception being Cuddalore. Hence, undercurrents are seen more off Cuddalore than off the other three locations (figure 11). As in the seasonal bands, the phase tends to propagate upward in the 30–90-day band, leading to a patchy coherence between the 48 m ADCP current and the OSCAR current (figure 4). The ADCP-OSCAR coherence is high during 2013–2014 off Visakhapatnam and Kakinada and 2014–2015 off Cuddalore.

Variability in the 4–30-day band is also evident at all four locations (figure 6). While the variability in this band also shows seasonal variation and tends to be stronger during spring and winter, this is not true of all years at all locations. Though weak, variability in the 8–12-day band, which was noted on the west-coast slope (Amol *et al.* 2014) and east-coast slope (Mukherjee *et al.* 2014), is seen in the longer data record, but without a clear seasonal signal. As expected, this band also decorrelates along the coast (figure 10).

5.2 *Interannual variability*

There are two ways of analysing interannual variability. The first approach, which examines the variability of the annual and higher frequencies (seasonal and intraseasonal variability) across years, has been dealt in sections 4 and 5.1, which dealt with the seasonal cycle and intraseasonal variability, respectively. The second approach, adopted here, analyses the sub-annual variability using a low-pass Lanczos filter. The wavelet power spectrum suggests that variability at periods of the order of 512 days (just under 1.5 yrs) or more is present at all the four mooring locations. (Following Mukherjee *et al.* (2014), we use *suggests* instead of *shows* for the sub-annual variability owing to much of the time series lying outside the cone of influence at these periods.) We use a 500-day low-pass Lanczos filter to estimate the sub-annual current; the weighting window is $1.5/f_2$, as done earlier for the annual band.

The 500-day low-passed EICC is not weak: the magnitude exceeds $20\,\mathrm{cm\,s^{-1}}$ over a part of the time series at all locations and it exceeds $30\,\mathrm{cm\,s^{-1}}$ off Gopalpur and Kakinada in 2010 and off Visakhapatnam in 2016 (figure 12). Data gaps and the later start of the time series off Visakhapatnam narrows the number of years for which we have valid data in the sub-annual band. The 500-day low-passed OSCAR current matches the ADCP current off Gopalpur, Visakahapatnam, and Kakinada, suggesting that the sub-annual EICC may have exceeded $30\,\mathrm{cm\,s^{-1}}$ off Visakhapatnam in 2010 and off Gopalpur in 2016. Off Cuddalore, though the variability of the sub-annual OSCAR current matches that of the ADCP current at 48 m, it shows a negative (equatorward) bias of $\sim 20\,\mathrm{cm\,s^{-1}}$ with respect to the ADCP current. The EICC oscillates about zero in the ADCP data, but flows equatorward almost throughout the time series in the OSCAR data. Nevertheless, the close match between the variability observed in both ADCP and OSCAR currents suggests that there is significant sub-annual variability in the regime of the EICC.

Plotting the 500-day-low-passed alongshore EICC as a function of time and latitude (figure 12) shows pockets of both equatorward and poleward flow in certain years, with the equatorward (poleward) flow tending to dominate more in the northern and southern (central) bay. For example, there is a sub-annual poleward flow during the spring and summer of 2010–2012 in the northern and central bay from just south off Gopalpur to just south of Kakinada. Another such episode occurs in 2014, but the poleward flow extends farther north this year. Likewise, there is strong equatorward flow south of roughly 14°N during the winter (October–December) of 2010, 2013, and 2016–2017; the peak of this equatorward flow tends to occur in November. The lack of alongshore coherence suggests that the sub-annual EICC decorrelates along the Indian east coast, as noted in the altimeter data by Durand *et al.* (2009). Other studies have also noted the existence of eddies at interannual time scales in the western bay (Chen *et al.* 2012) and the existence of these eddies, whose spatial scale is much less than that of the coast, is expected to lead to an alongshore decorrelation even at these time scales.

6. Discussion

To summarise, the longer data record, roughly nine years long (2009–2018), allows us to attach a statistically more robust basis to the conclusions

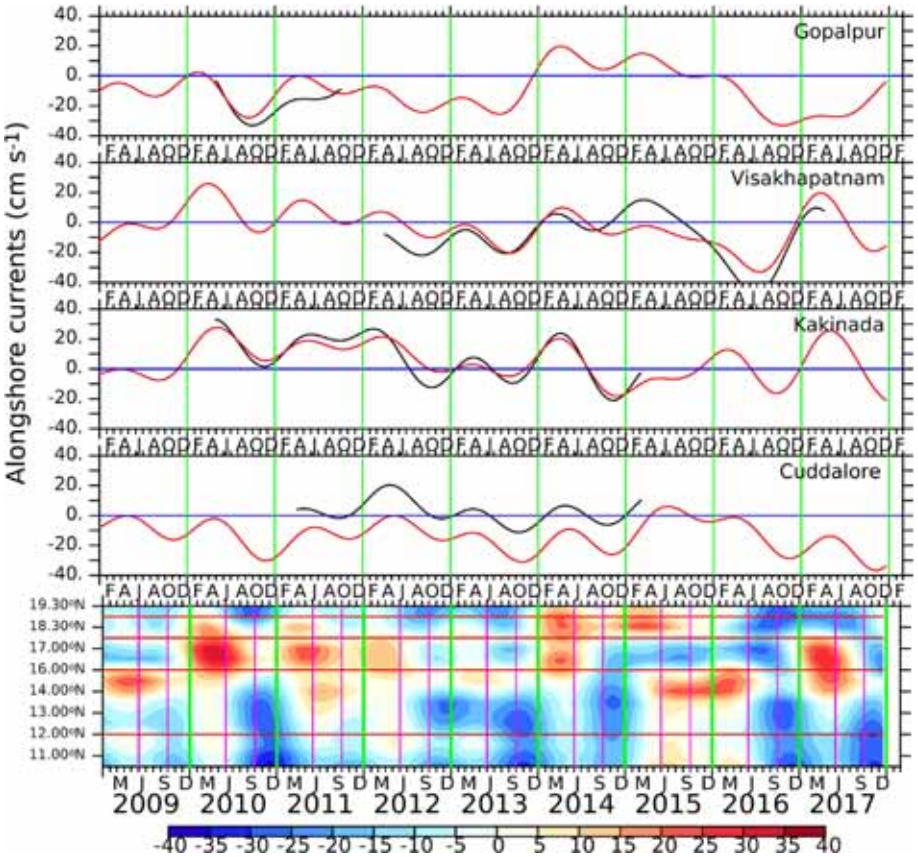

Figure 12. Sub-annual variability of the alongshore current (cm s^{-1}). The top four panels show the 500-day-low-passed alongshore current estimated using a Lanczos filter from the ADCP (black curves) and OSCAR (red curves) data at the four mooring locations. As in figure 4, the ADCP current is at 48 m and the grid point nearest the mooring location was used for the OSCAR current. The bottom panel shows the 500-day-low-passed alongshore OSCAR current as a function of time (abscissa) and latitude (ordinate). The horizontal red lines mark the latitude of the ADCP mooring locations. In all eight panels, the vertical green lines are used to separate the years.

drawn by Mukherjee *et al.* (2014) on the basis of four years (2009–2013) of ADCP data. In spite of data gaps, the longer record available off Gopalpur in the northern bay, Visakhapatnam and Kakinada in the central bay, and Cuddalore in the southern bay confirms that the seasonal cycle dominates the variability of the EICC (figures 6, 7, 9, 11). The amplitude of the annual band varies over the time series (figures 6, 9). In the intra-annual band, the variability switches between the semi-annual and 120-day bands off Gopalpur, Visakhapatnam and Kakinada, but the semi-annual band is stronger than the 120-day band off Cuddalore throughout the time series (figures 6, 7, 11). Upward phase propagation is common in the seasonal bands, but downward phase propagation is common in the intra-annual band off Cuddalore; it was noted during 2010 by Mukherjee *et al.* (2014), but the longer record shows it is a common feature in the southeastern bay during the summer and winter monsoons, leading to stronger undercurrents off Cuddalore (figure 11). Off Cuddalore, even the annual EICC appears as a shallow current (figure 9). In contrast, the EICC appears as a deep flow off Gopalpur, Visakhapatnam, and Kakinada particularly during the spring inter-monsoon (figure 11). This deep flow is evident at these locations even in the intraseasonal (30–90-day) band. The longer data set suggests, however, that the intraseasonal variability is not restricted to spring (figures 6, 11), implying that the inference of Mukherjee *et al.* (2014) based on the shorter data record is not valid. Off Cuddalore, the intraseasonal EICC is shallow, leading to stronger undercurrents. As noted in earlier studies, including Mukherjee *et al.* (2014), the annual EICC is coherent along the coast, but it is only the semi-annual band that shows a comparable coherence between Kakinada and Cuddalore: in the 120-day and intraseasonal bands, the EICC decorrelates along the coast (figure 10).

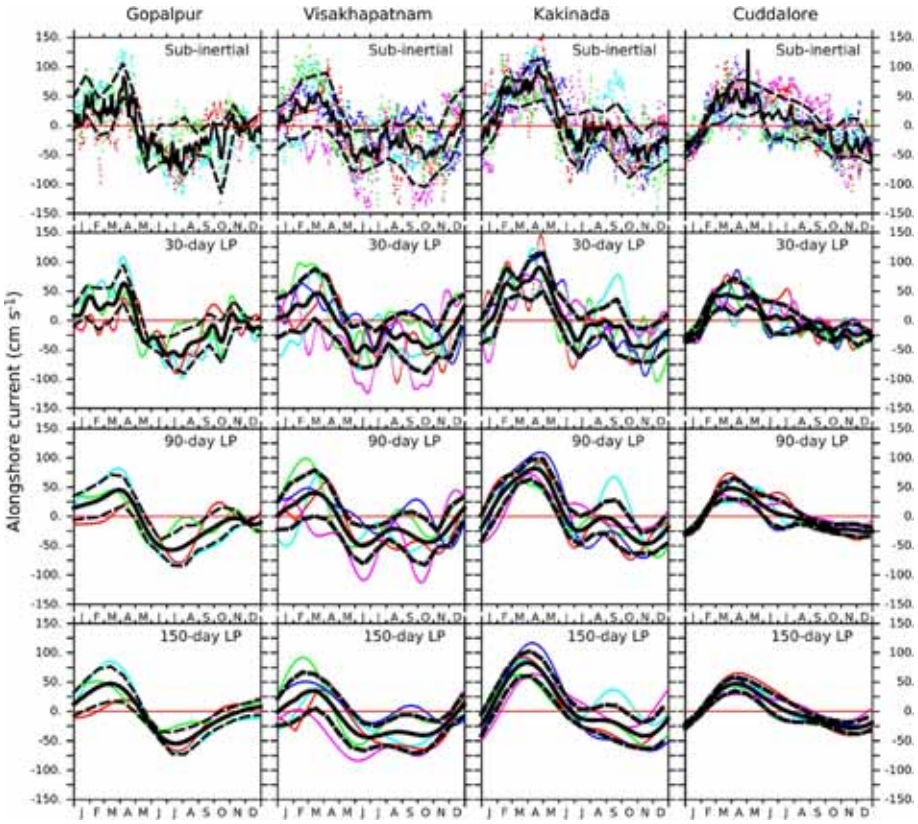

Figure 13. In which direction does the alongshore EICC flow on a given day? The top panels show the alongshore, sub-inertial EICC ($cm\,s^{-1}$) at 48 m the four mooring locations. The solid black curve is the mean for the available data during 2009–2018 and each colour represents the current during a particular year. The dashed black curves mark one standard deviation about the mean. The panels in the second, third, and fourth rows show the 30-day, 90-day, and 150-day low-passed (LP) current; the Lanczos filter was used for filtering and the solid and dashed black curves and the coloured dots are as in the top panels. Note that in spite of the scatter of the coloured dots about the mean, the canonical poleward (equatorward) direction of the EICC is evident even in the sub-inertial current in the top panels. It is only during summer, when the near-surface EICC is weak, that the scatter about the zero line is significant, indicating the possibility that the EICC may flow in either direction during a given year.

Wavelet analysis suggests significant variability at sub-annual periods (figure 6), which is confirmed by analysing the 500-day-low-passed alongshore current in the ADCP and OSCAR data (figure 12). The sub-annual EICC exceeds $20\,cm\,s^{-1}$ on many occasions. There are years in which the sub-annual EICC is strong, with poleward flow tending to be more common in the central bay and equatorward flow in the northern and southern bay. As noted in earlier studies, the interannual EICC also decorrelates along the coast (figure 10). Studies have shown the impact of the major climate modes like ENSO (El Niño and the Southern Oscillation) and the Indian-Ocean Dipole (IOD; Saji *et al.* 1999; Webster *et al.* 1999), on the EICC and the sea level along the Indian east coast (Clarke and Liu 1994; Shankar 1998; Shankar and Shetye 1999; Schott and McCreary 2001; Han and Webster 2002; Srinivas *et al.* 2005; Durand *et al.* 2009; Vialard *et al.* 2009; Schott *et al.* 2009; Aparna *et al.* 2012; Chen *et al.* 2012; Sreenivas *et al.* 2012; Suresh *et al.* 2013; Sherin *et al.* 2018; Mukherjee and Kalita 2019). While it is tempting to interpret the peaks in interannual variability in terms of the major climate modes like ENSO (El Niño and the Southern Oscillation) and the Indian-Ocean Dipole (IOD; Saji *et al.* 1999; Webster *et al.* 1999), we refrain from doing so because the data gaps preclude firm conclusions on the basis of the ADCP data alone: a more detailed study that uses the ADCP data in conjunction with OSCAR data is desirable because studies have shown the impact of these climate modes on the EICC and the sea level along the Indian east coast (Clarke and Liu 1994; Shankar 1998; Shankar and Shetye 1999; Schott and McCreary 2001; Han and Webster 2002; Srinivas *et al.* 2005; Durand *et al.* 2009; Vialard *et al.* 2009; Schott *et al.* 2009; Aparna *et al.* 2012;

Chen *et al.* 2012; Sreenivas *et al.* 2012; Suresh *et al.* 2013; Sherin *et al.* 2018; Mukherjee and Kalita 2019), but is not attempted here.

The long ADCP record allows us to confirm the dominance of seasonality in the EICC regime in a robust fashion. To do so, we ask the following question. On a given day of the year, say 21 March, in which direction will the EICC flow? The panels for sub-inertial flow in figure 13 show that the direction in spring (winter) is almost always poleward (equatorward), but the winter peak occurs earlier (October) off Gopalpur in the northern bay than in the southern bay, where it tends to occur during November. This north–south change in the peak of the equatorward EICC has been noted even in tide-gauge and ship-drift data (Shankar 1998, 2000). It is only during the summer monsoon, when the remote forcing by interior Ekman pumping and from the equatorial Indian Ocean opposes the strong poleward EICC forced by the local alongshore winds (Shankar *et al.* 1996; McCreary *et al.* 1996; Vinayachandran *et al.* 1996), that the direction of the EICC is ambiguous, with the scatter around the mean tending to lie on both sides of the zero line (figure 13). Applying a 30-day low-pass filter is sufficient, however, to establish that seasonal variability dominates in the regime of the EICC. This dominance of seasonality is in striking contrast to the dominance of intraseasonal variability in the regime of the WICC (Amol *et al.* 2014), for which a similar analysis suggests that the WICC can flow in either direction on a given day of the year (Chaudhuri *et al.* 2020). This dominance of seasonality enhances the predictability of the EICC.

The ADCP measurements are continuing and new moorings have been added to the network. One mooring has been deployed between Cuddalore and Kakinada and another on the continental slope off the northern bay (figure 1). This expansion of the network and the standardization of the mooring layout to include a 153 kHz ADCP at ∼150–200 m and a second ADCP of 76 kHz at ∼400 m will allow a more complete time series to be established over the top ∼400 m of the water column in the regime of the EICC. The use of the 153 kHz ADCP will also permit sampling up to ∼20 m from the surface, which is useful in view of the shallow mixed layers that prevail in the western bay (Shetye *et al.* 1991, 1996; Chatterjee *et al.* 2012). As noted by Mukherjee *et al.* (2018) and Mukherjee and Kalita (2019), however, models need considerable improvement to enable them to simulate accurately the intra-annual and intraseasonal variability of the EICC being revealed by these ADCP measurements.

Acknowledgements

The ADCP mooring project has been supported by grants from the Council of Scientific and Industrial Research (CSIR) (under the Supra-Institutional Program of CSIR-NIO during 2007–2012, under OCEAN FINDER during 2012–2017, and TRIM-Fish thereafter) and the Ministry of Earth Sciences (MoES, via INCOIS) through its programme on Ocean Observing Networks. The support from INCOIS, the CSIR-NIO ship cell, and the officers and crew on board the research vessels are acknowledged with gratitude. S Mukhopadhyay was supported earlier by funds from CSIR and is currently supported by funds from MoES. Critical comments from two anonymous reviewers helped improve the paper. Ferret has been used for analysis and Ferret and GMT (Generic Mapping Tools) have been used for graphics; the FORTRAN code for wavelet analysis and the *R* package for wavelet coherence spectra were downloaded from http://paos.colorado.edu/research/wavelets and http://tocsy.agnld.uni-potsdam.de/wavelets, respectively. This is CSIR-NIO contribution 6475 and INCOIS contribution 361.

References

Amol P 2014 Intraseasonal variability of currents along west coast of India; Ph.D. thesis, Goa University, India.

Amol P, Shankar D, Aparna S G, Shenoi S S C, Fernando V, Shetye S R, Mukherjee A, Agarvadekar Y, Khalap S T and Satelkar N P 2012 Observational evidence from direct current measurements for propagation of remotely forced waves on the shelf off the west coast of India; *J. Geophys. Res.* **117**, https://doi.org/10.1029/2011JC007606.

Amol P, Shankar D, Fernando V, Mukherjee A, Aparna S G, Fernandes R, Michael G S, Khalap S T, Satelkar N P, Agarvadekar Y, Gaonkar M G, Tari A P, Kankonkar A and Vernekar S P 2014 Observed intraseasonal and seasonal variability of the West India Coastal Current on the continental slope; *J. Earth Syst. Sci.* **123** 1045–1074, https://doi.org/10.1007/s12040-014-0449-5.

Aparna S G , McCreary J P, Shankar D and Vinayachandran P N 2012 Signatures of the Indian Ocean Dipole and EI Niño-Southern Oscillation events in sea level variations in the Bay of Bengal; *J. Geophys. Res.* **117**, https://doi.org/10.1029/2012JC008055.

Bell C, Vassie J M and Woodworth P L 1998 POL/PSMSL Tidal Analysis Software Kit 2000 TASK-2000). Tech. rep., Permanent Service for Mean Sea Level, UK.

Bonjean F and Lagerloef G S E 2002 Diagnostic model and analysis of the surface currents in the tropical Pacific Ocean; *J. Phys. Oceanogr.* **32** 2938–2954, https://doi.org/10.1175/1520-0485(2002)032<2938:DMAAOT>2.0.CO;2.

Chatterjee A, Shankar D, Shenoi S S C, Reddy G V, Michael G S, Ravichandran M, Gopalkrishna V V, Rao E P R, Bhaskar T V S U and Sanjeevan V N 2012 A new atlas of temperature and salinity for the north Indian Ocean; *J. Earth Syst. Sci.* **121** 559–593, https://doi.org/10.1007/s12040-012-0191-9.

Chaudhuri A, Shankar D, Aparna S G, Amol P, Fernando V, Kankonkar A, Michael G S, Satelkar N P, Khalap S T, Tari A P, Gaonkar M G, Ghatkar S and Khedekar R R 2020 Observed variability of the West India Coastal Current on the continental slope from 2009–2018; *J. Earth Syst. Sci.* **129** 57, https://doi.org/10.1007/s12040-019-1322-3.

Chen G, Wang D and Hou Y 2012 The features and interannual variability mechanism of mesoscale eddies in the Bay of Bengal; *Cont. Shelf Res.* **47** 178–185, https://doi.org/10.1016/j.csr.2012.07.011.

Cheng X, Xie S P, McCreary J P, Qi Y and Du Y 2013 Intraseasonal variability of sea surface height in the Bay of Bengal. *J. Geophys. Res.* **118** 816–830, https://doi.org/10.1002/jgrc.20075.

Clarke A J and Liu X 1994 Interannual sea level in the northern and eastern Indian Ocean; *J. Phys. Oceanogr.* **24** 1224–1235.

Cutler A N and Swallow J C 1984 Surface currents of the Indian ocean (to 25°S, 100°E): Compiled from historical data archived by the Meteorological Office, Bracknell, UK; Tech. rep., Metorological Office, UK.

Durand F, Shankar D, Birol F and Shenoi S 2009 Spatiotemporal structure of the East India Coastal Current from satellite altimetry; *J. Geophys. Res.* **114**, https://doi.org/10.1029/2008JC004807.

Eigenheer A and Quadfasel D 2000 Seasonal variability of the Bay of Bengal circulation inferred from TOPEX/Poseidon altimetry; *J. Geophys. Res.* **105** 3243–3252, https://doi.org/10.1029/1999JC900291.

Girishkumar M, Ravichandran M and Han W 2013 Observed intraseasonal thermocline variability in the Bay of Bengal; *J. Geophys. Res.* **118** 3336–3349, https://doi.org/10.1002/jgrc.20245.

Han W and Webster P 2002 Forcing mechanisms of sea level inter-annual variability in the Bay of Bengal; *J. Phys. Oceanogr.* **32** 216–239, https://doi.org/10.1175/1520-0485(2002)032<0216:FMOSLI>2.0.CO;2.

Han W, McCreary J P, Masumoto Y, Vialard J and Duncan B 2011 Basin resonances in the equatorial Indian Ocean; *J. Phys. Oceanogr.* **41** 1252–1270, https://doi.org/10.1175/2011JPO4591.1.

Kurien P, Ikeda M and Valsala V K 2010 Mesoscale variability along the east coast of India in spring as revealed from satellite data and OGCM simulations; *J. Oceanogr.* **66** 273–289, https://doi.org/10.1007/s10872-010-0024-x.

Kutsuwada K and McPhaden M 2002 Intraseasonal variations in the upper equatorial Pacific Ocean prior to and during the 1997–1998 El Niño; *J. Phys. Oceanogr.* **32** 1133–1149, https://doi.org/10.1175/1520-0485(2002)032<1133:IVITUE>2.0.CO;2.

Legeckis R 1987 Satellite observations of a western boundary current in the Bay of Bengal; *J. Geophys. Res.* **92** 12,974–12,978.

Madden R A and Julian P R 1971 Detection of a 40–50 day oscillation in the zonal wind of the tropical Pacific; *J. Atmos. Sci.* **28** 702–708.

Madden R A and Julian P R 1972 Description of global-scale circulation cells in the tropics with a 40–50 day period; *J. Atmos. Sci.* **29** 1109–1123.

Maraun D and Kurths J 2004 Cross-wavelet analysis: Significance testing and pitfalls; *Nonlinear Process. Geophys.* **11** 505–514, https://doi.org/10.5194/npg-11-505-2004.

Mariano A J, Ryan E H, Perkins B D and Smithers S 1995 The Mariano Global Surface Velocity Analysis 1.0; USCG Report CG-D-34-95, Office of Engineering, Logistics, and Development, United States Coast Guard.

McCreary J P, Kundu P K and Molinari R L 1993 A numerical investigation of dynamics, thermodynamics and mixed-layer processes in the Indian Ocean; *Prog. Oceanogr.* **31** 181–244, https://doi.org/10.1016/0079-6611(93)90002-U.

McCreary J P, Han W, Shankar D and Shetye S R 1996 Dynamics of the East India Coastal Current 2. Numerical solutions; *J. Geophys. Res.* **101** 13,993–14,010, https://doi.org/10.1029/96JC00560.

Mukherjee A 2017 Intraseasonal variability of currents along east coast of India; Ph.D. thesis, Goa University, India.

Mukherjee A and Kalita B 2019 Signature of La Niña in interannual variations of the East India Coastal Current during spring; *Clim. Dyn.* **52** 1–18, https://doi.org/10.1007/s00382-018-4601-9.

Mukherjee A, Shankar D, Aparna S G, Amol P, Fernando V, Fernandes R, Khalap S T, Narayan S, Agarvadekar Y, Gaonkar M G, Tari A P, Kankonkar A and Vernekar S P 2013 Near-inertial currents off the east coast of India; *Cont. Shelf Res.* **55** 29–39, https://doi.org/10.1016/j.csr.2013.01.007.

Mukherjee A, Shankar D, Fernando V, Amol P, Aparna S G, Fernandes R, Michael G S, Khalap S T, Satelkar N P, Agarvadekar Y, Gaonkar M G, Tari A P, Kankonkar A and Vernekar S P 2014 Observed seasonal and intraseasonal variability of the East India Coastal Current on the continental slope; *J. Earth Syst. Sci.* **123** 1197–1232, https://doi.org/10.1007/s12040-014-0471-7.

Mukherjee A, Shankar D, Chatterjee A and Vinayachandran P N 2018 Numerical simulation of the observed near-surface East India Coastal Current on the continental slope; *Clim. Dyn.* **50** 3949–3980, https://doi.org/10.1007/s00382-017-3856-x.

Mukhopadhyay S, Shankar D, Aparna S G and Mukherjee A 2017 Observations of the sub-inertial, near-surface East India Coastal Current; *Cont. Shelf Res.* **148** 159–177, https://doi.org/10.1016/j.csr.2017.08.020.

Nethery D and Shankar D 2007 Vertical propagation of baroclinic Kelvin waves along the west coast of India; *J. Earth Syst. Sci.* **116** 331–339, https://doi.org/10.1007/s12040-007-0030-6.

Nuncio M and Kumar S P 2012 Life cycle of eddies along the western boundary of the Bay of Bengal and their implications; *J. Mar. Syst.* **94** 9–17, https://doi.org/10.1016/j.jmarsys.2011.10.002.

Potemra J T, Luther M E and O'Brien J J 1991 The seasonal circulation of the upper ocean in the Bay of Bengal; *J. Geophys. Res.* **96** 12,667–12,683, https://doi.org/10.1029/91JC01045.

Saji N H, Goswami B N, Vinayachandran P N and Yamagata T 1999 A dipole mode in the tropical Indian Ocean; *Nature* **401** 360–363.

Schott F A and McCreary J P 2001 The monsoon circulation of the Indian Ocean; *Prog. Oceanogr.* **51** 1–123, https://doi.org/10.1016/S0079-6611(01)00083-0.

Schott F A, Xie S and McCreary J P 2009 Indian Ocean circulation and climate variability; *Rev. Geophys.* **47**, https://doi.org/10.1029/2007RG000245.

Shankar D 1998 Low-frequency variability of sea level along the coast of India; Ph.D. thesis, Goa University, India.

Shankar D 2000 Seasonal cycle of sea level and currents along the coast of India; *Curr. Sci.* **78** 279–288.

Shankar D and Shetye S R 1999 Are interdecadal sea level changes along the Indian coast influenced by variability of monsoon rainfall? *J. Geophys. Res.* **104** 26,031–26,042, https://doi.org/10.1029/1999JC900218.

Shankar D, McCreary J P, Han and Shetye S R 1996 Dynamics of the East India Coastal Current 1. Analytic solutions forced by interior Ekman pumping and local alongshore winds; *J. Geophys. Res.* **101** 13,975–13,991, https://doi.org/10.1029/96JC00559.

Shankar D, Vinayachandran P N and Unnikrishnan A S 2002 The monsoon currents in the north Indian Ocean; *Prog. Oceanogr.* **52** 63–120, https://doi.org/10.1016/S0079-6611(02)00024-1.

Shenoi S, Shankar D and Shetye S R 2002 Differences in heat budgets of the near-surface Arabian Sea and Bay of Bengal: Implications for the summer monsoon; *J. Geophys. Res.* **107**, https://doi.org/10.1029/2000JC000679.

Sherin V, Durand F, Gopalkrishna V, Anuvinda S, Chaitanya A, Bourdallé-Badie R and Papa F 2018 Signature of Indian Ocean Dipole on the western boundary current of the Bay of Bengal; *Deep-Sea Res. I* **136** 91–106, https://doi.org/10.1016/j.dsr.2018.04.002.

Shetye S, Shenoi S, Gouveia A, Michael G, Sundar D and Nampoothiri G 1991 Wind-driven coastal upwelling along the western boundary of the Bay of Bengal during the southwest monsoon; *Cont. Shelf Res.* **11** 1397–1408, https://doi.org/10.1016/0278-4343(91)90042-5.

Shetye S R and Gouveia A D 1998 Coastal circulation in the north Indian Ocean: Coastal segment (14, SW); In: *The Sea*, (ed.) Robinson A R, John Wiley and Sons, New York, USA, pp. 523–556.

Shetye S R, Gouveia A D, Shenoi S S C, Sundar D, Michael G S and Nampoothiri G 1993 The western boundary current of the seasonal subtropical gyre in the Bay of Bengal; *J. Geophys. Res.* **98** 945–954, https://doi.org/10.1029/92JC02070.

Shetye S R, Gouveia A D, Shankar D, Shenoi S S C, Vinayachandran P N, Sundar D, Michael G S and Nampoothiri G 1996 Hydrography and circulation in the western Bay of Bengal during the northeast monsoon. *J. Geophys. Res.* **101** 14,011–14,025, https://doi.org/10.1029/95JC03307.

Sreenivas P, Gnanaseelan C and Prasad K V S R 2012 Influence of EI Niño and Indian Ocean Dipole on sea level variability in the Bay of Bengal; *Glob. Planet. Change* **80–81** 215–225, https://doi.org/10.1016/j.gloplacha.2011.11.001.

Srinivas K, Kumar P K D and Revichandran C 2005 ENSO signature in the sea level along the coastline of the Indian subcontinent; *Ind. J. Mar. Sci.* **34** 225–236.

Suresh I, Vialard J, Lengaigne M, Han W, McCreary J, Durand F and Muraleedharan P M 2013 Origins of wind-driven intraseasonal sea level variations in the north Indian Ocean coastal waveguide; *Geophys. Res. Lett.* **40** 5740–5744.

Torrence C and Compo G P 1998 A practical guide to wavelet analysis; *Bull. Amer. Meteorol. Soc.* **79** 61–78, https://doi.org/10.1175/1520-0477(1998)079<0061:APGTWA>2.0.CO;2.

Varkey M, Murty V and Suryanarayana A 1996 Physical oceanography of the Bay of Bengal and Andaman Sea; *Oceanogr. Mar. Biol.* **34** 1–70.

Vialard J, Shenoi S S C, McCreary J P, Shankar D, Durand F, Fernando V and Shetye S R 2009 Intraseasonal response of the northern Indian Ocean coastal waveguide to the Madden–Julian oscillation; *Geophys. Res. Lett.* **36**, https://doi.org/10.1029/2009GL038450.

Vinayachandran P N, Shetye S R, Sengupta D and Gadgil S 1996 Forcing mechanisms of the Bay of Bengal circulation. *Curr. Sci.* **71** 753–763.

Webster P J, Moore A M, Loschnigg J P and Leben R R 1999 Coupled ocean-atmosphere dynamics in the Indian Ocean during 1997–1998; *Nature* **401** 356–360.

Yu L, O'Brien J J and Yang J 1991 On the remote forcing of the circulation in the Bay of Bengal *J. Geophys. Res.* **96** 20449–20454, https://doi.org/10.1029/91JC02424.

Corresponding editor: C Gnanaseelan